LANGMUIR

pubs.acs.org/Langmuir Article

Structural Engineering in the Self-Assembly of Amphiphilic Block Copolymers with Reactive Additives: Micelles, Vesicles, and Beyond

Lei Jin, Chung-Hao Liu, Daniel Cintron, Qiang Luo, Mu-Ping Nieh, and Jie He*

Cite This: Langmuir 2021, 37, 9865−9872 Read Online

ACCESS | Metrics & More | Article Recommendations | Supporting Information

ABSTRACT: Control of polymer assemblies in solution is of great importance to determine the properties and applications of these polymer nanostructures. We report a novel co-self-assembly strategy to control the self-assembly outcomes of a micelle-forming amphiphilic block copolymer (BCP) of poly(ethylene oxide) (PEO) and poly[3-(trimethoxysilyl)propyl methacrylate] (PTMSPMA), PEO_{114}-b-$PTMSPMA_{228}$. With a reactive and hydrophobic additive tetraethyl orthosilicate (TEOS), the assembly nanostructures of PEO_{114}-b-$PTMSPMA_{228}$ are tunable. The swelling of the PTMSPMA block by hydrophobic TEOS increases the hydrophobic-to-hydrophilic ratio that enables a continuous morphological evolution from spherical micelles to vesicles and eventually to large compound vesicles. TEOS that co-hydrolyzes with the PTMSPMA block can further stabilize and fix these hybrid nanostructures. With high TEOS concentrations, these polymer assemblies can be further converted through thermal annealing into unique silica nanomaterials, including nanospheres, hollow nanoparticles with dual shells, and mesoporous silica frameworks that cannot be synthesized through conventional syntheses otherwise.

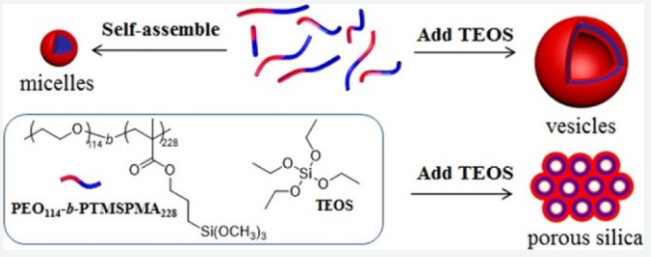

1. INTRODUCTION

The self-assembly of amphiphilic block copolymers (BCPs) has attracted broad interest due to their unique and useful nanostructures for many technical applications.[1] As so-called "soft" templates, amphiphilic BCPs are of particular importance to design porous materials such as metal oxides and carbons.[2−5] In these syntheses, BCPs in the form of micelles usually interact with precursors (e.g., metal salts for porous metal oxides) to assemble into an ordered liquid crystal phase. The hydrophilic block, e.g., poly(ethylene oxide) (PEO), can interact with metal salts through a weak coordination to form porous frameworks; while the hydrophobic block is often sacrificial to generate pores. Although the hydrophobic-to-hydrophilic balance of amphiphilic BCPs is critical,[6] these mesoporous structures are also influenced by the inorganic−template hybrid interface that involves an interaction between the solvent, template, and inorganic precursors during the typical evaporation-induced self-assembly process.[7]

Amphiphilic BCPs have abundant nanostructures in aqueous solution similar to small molecular amphiphiles.[1] Control of their self-assembly outcomes is determined by the packing parameter (P), $P = v_c/(a_o l_c)$, where v_c is the volume of the hydrophobic portions, a_o is the cross-sectional area of the hydrophilic portions at the aggregate interface, and l_c is the length of the hydrophobic chain. With the increase of the packing parameter, the self-assembly of amphiphilic BCPs undergoes morphological transitions from spherical micelles to cylindrical micelles, to vesicles, to planar bilayers, and eventually to inverted structures.[8] With advances in synthetic methodologies, the micellar structures of BCPs are possibly customized with a precise chemical composition for any targeted applications, as demonstrated in the pioneering works of Eisenberg and Zhang.[9,10] Self-assembly of amphiphilic BCPs can also be tuned by additives.[11] The key mechanism is to tune the interaction of solvent and BCPs (i.e., either hydrophilic or hydrophobic block). In the case of polystyrene-b-poly(acrylic acid) (PS-b-PAA), the solution aggregates of the same block ratio can be varied by addition of ions, such as HCl and NaCl.[11] The gradual decrease of the ionic repulsion among the PAA blocks could show a full diagram of structures that are conventionally required with new polymers with different compositions. On the other hand, a more straightforward method is to vary the volume fraction of the two blocks using additives. This concept has been practiced in the control over the phase separation diagram of BCPs in the solid state. Adding a homopolymer that enthalpically interacts only with one phase, i.e., concurrent self-assembly of the homopolymer and BCP, can vary the volume fraction of the two blocks;[12−14] thus, it varies the nanostructure of phase separation. Similarly,

Received: June 9, 2021
Revised: July 13, 2021
Published: August 5, 2021

https://doi.org/10.1021/acs.langmuir.1c01554
Langmuir 2021, 37, 9865−9872

Scheme 1. Scheme for Structural Engineering in the Self-Assembly of the Micelle-Forming PEO-b-PTMSPMA to Vesicles and Porous Large Compound Vesicles with Excess TEOS

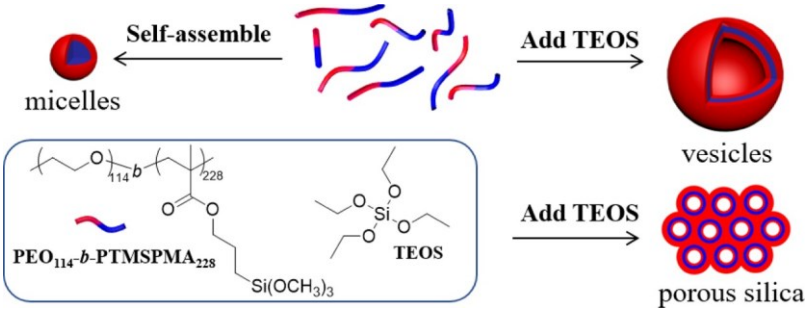

this method can be applied to other additives such as small molecules or nanoparticles that interact with one phase in BCPs.[15−19] However, adding hydrophobic homopolymers to amphiphilic BCPs in solution does not contribute to the structural evolution of micelles. The likely reason is the difference in critical micelle concentrations between hydrophobic homopolymers and amphiphilic BCPs.[20] Upon addition of a poor solvent, homopolymers collapse first, while the amphiphilic BCPs serve as surfactants to stabilize the aggregates. Although there are successful examples of adding hydrophobic additives that strongly interact with BCPs through hydrogen bonding,[21] those strategies only work for very specific BCPs and additives.

Amphiphilic BCPs containing a reactive block such as poly[3-(trimethoxysilyl)propyl methacrylate] (PTMSPMA) have very promising applications to design hybrid polymer nanostructures.[22−25] Upon assembly, the hydrolysis of trimethoxysilyl moieties can lead to the formation of silica-like polysilsesquioxane structures with Si−O−Si bonds. Our group has demonstrated the use of amphiphilic BCPs, PEO-b-PTMSPMA, to synthesize crystalline mesoporous metal oxides.[26−32] These BCPs as soft templates allow the crystallization of complex oxides up to 1000 °C because of the remarkable stability of these hybrid polymers after the conversion to inorganic silica. However, given their reactivity with moisture, the control over the nanostructures of PTMSPMA-containing BCPs is more difficult to handle compared to conventional BCPs, including the size control of those polymer micelles. Herein, we report a new method to tune the self-assembly nanostructures of PEO-b-PTMSPMA using a reactive additive, tetraethyl orthosilicate (TEOS). TEOS shares a similar ethoxysilyl group and it can co-assemble with the PTMSPMA block in the mixture of ethanol and water. As it swells the hydrophobic PTMSPMA domain, the addition of TEOS varies the volume fraction of PEO-b-PTMSPMA. With the increase of TEOS in the micelle-forming PEO_{114}-b-$PTMSPMA_{228}$, the morphological transition from spherical micelles to vesicles and large compound vesicles, and eventually to bicontinuous mesophases (Scheme 1) takes place, in alignment with the volume increase of the hydrophobic block. The co-hydrolysis of TEOS and PTMSPMA allows further stabilization of those hierarchical nanostructures. We demonstrate the conversion of those solution aggregates further into silica nanomaterials in the form of nanoparticles, hollow nanospheres, and mesoporous silica.

2. EXPERIMENTAL SECTION

2.1. Amphiphilic BCP of PEO_{114}-b-$PTMSPMA_{228}$. The amphiphilic BCP of PEO_{114}-b-$PTMSPMA_{228}$ (M_n = 61.7 kg mol^{-1}, $Đ$ = 1.3) was prepared through atom-transfer radical polymerization (ATRP), as reported previously (see Figure S1).[33] The block ratio was characterized by proton nuclear magnetic resonance (^{1}H NMR) spectroscopy and gel permeation chromatography (GPC). The as-prepared PEO_{114}-b-$PTMSPMA_{228}$ was dissolved and stored in anhydrous ethanol at a concentration of 20 mg mL^{-1} for further use.

2.2. Self-Assembly of PEO_{114}-b-$PTMSPMA_{228}$. The self-assembly of PEO_{114}-b-$PTMSPMA_{228}$ was carried out in the mixture solvent of water/ethanol. In a typical procedure, 1 mL of ethanol solution of BCP (20 mg mL^{-1}) was diluted with 1 mL of ethanol, followed by dropwise addition of 2.4 mL of water in 30 min. After stirring for half an hour, 0.2 mL of triethylamine (TEA) was added to the solution mixture to catalyze the hydrolysis and condensation of the PTMSPMA block. The solution was kept stirring for 24 h and it was then dialyzed against water overnight to remove ethanol.

For TEOS-directed self-assembly, the experiments were carried out similarly. Typically, 1 mL of BCP solution was diluted with 1 mL of ethanol containing a predetermined amount of TEOS. After stirring for 1 h, 2.4 mL of water was added dropwise around 30 min. The solution was further stirred for another 30 min before 0.2 mL of TEA was added to catalyze the hydrolysis and condensation of the PTMSPMA block and TEOS. The mixture was kept stirring for 24 h and it was then dialyzed against water overnight to remove ethanol. We varied the amount of TEOS in the range of 0.01−0.8 mL. The details of those samples are summarized in Table 1.

2.3. Calcination. The micellar samples were further calcined to remove organic components in the assembled nanostructures. The aqueous solution of aggregates was first dried using a lyophilizer

Table 1. Summary of the Self-Assembly Conditions and Statistical Analysis of Polymer Micelles at Various TEOS Concentrations

sample no.[a]	TEOS (mL)	size (nm)	wall thickness (nm)[b]
Si-0	0	21.6 ± 2.8	
Si-1	0.01	22.3 ± 2.5	
Si-2	0.05	25.7 ± 2.4	
Si-3	0.1	29.6 ± 3.2	
Si-4	0.2	32.2 ± 4.1	
Si-5	0.23	39.3 ± 5.9	
Si-6	0.27	46.8 ± 7.1	14.6 ± 1.6
Si-7	0.3	60.4 ± 7.0	18.6 ± 1.9
Si-8	0.35		14.7 ± 2.0
Si-9	0.4		13.6 ± 2.0
Si-10	0.5		14.1 ± 1.7
Si-11	0.6		15.4 ± 1.9
Si-12	0.8		14.4 ± 1.6

[a]The initial polymer concentration was 10 mg/mL in ethanol. 2.4 mL of water was added to the polymer ethanol solution (2 mL). For all samples, 0.2 mL of TEA was added to hydrolyze the polymer micelles. [b]Wall thickness of vesicles.

https://doi.org/10.1021/acs.langmuir.1c01554
Langmuir 2021, 37, 9865−9872

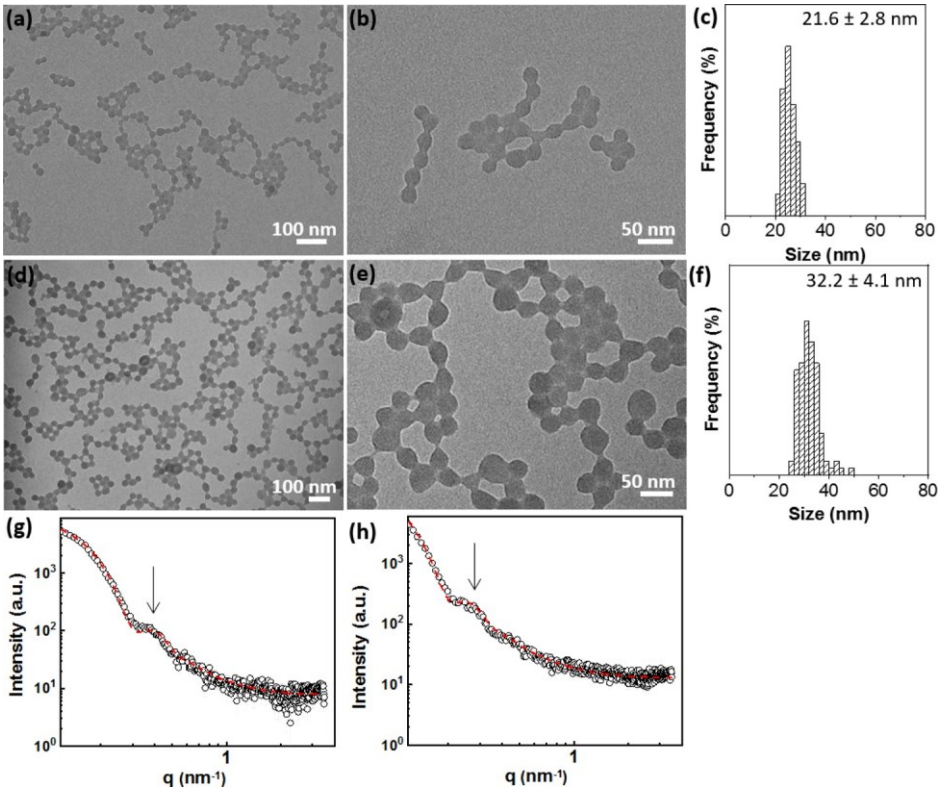

Figure 1. (a,b) TEM images and (c) size distribution of Si-0. (d,e) TEM images and (f) size distribution of Si-4. (g) SAXS profile of Si-0. (h) SAXS profile of Si-4.

(Labconco) to remove water. The as-resultant powder samples were then annealed in a tube furnace at 550 °C for 2 h under air. The final powder samples could be re-dispersed in water for electron microscopy imaging.

2.4. Other Characterization Methods. The ^{1}H NMR spectrum was measured using a Bruker Avance 400 mHz spectrometer. GPC was performed on a Waters GPC-1 (1515 HPLC pump and Waters 717Plus auto injector) equipped with a Varian 380-LC evaporative light-scattering detector, a Waters 2487 dual absorbance detector, and three Jordi gel fluorinated DVB columns (1−100 K, 2−10 K, and 1−500 Å). Tetrahydrofuran was used as the solvent at a flow rate of 1.25 mL min^{-1}. Polystyrene (PS) standards were used to calibrate the molecular weight and molecular-weight distribution. Transmission electron microscopy (TEM) was carried out using a FEI Tecnai 12 G2 Spirit BioTWIN microscope. The N_2 sorption isotherm was measured using a Quantachrome Autosorb-1-C automated nitrogen gas adsorption system.

Small-angle X-ray scattering (SAXS) measurements were performed using a Bruker Nano STAR instrument. The wavelength (λ) of 1.54 Å was generated by a Turbo (rotating anode) X-ray source. The sample-to-detector distance of 67 cm to cover a range of scattering vector, q from 0.012 to 0.35 Å^{-1}, where q is defined as $\frac{4\pi}{\lambda}\sin\left(\frac{\theta}{2}\right)$, and λ (1.542 Å) and θ are the wavelength and the scattering angle, respectively. Samples were loaded in the quartz capillaries and sealed with wax. The 2-D intensity data were collected by a MikroGap VÅNTEC-2000 detector (pixel size = 67 mm) and then corrected by the transmission and scattering contributions from the empty beam (in the absence of sample), followed by the circular average with respect to the beam center to yield 1-D profiles.

The static light-scattering (SLS) experiments were conducted using an ALV compact goniometer system with multidetectors (CGS-3MD, Germany) and λ of the He−Ne laser beam was 632.8 nm. The concentration, c, of each sample was 0.5 mg/mL, 0.25 mg/mL, and 0.125 mg/mL, respectively. The scattering intensity was measured at 25 °C with θ ranging from 26 to 140°. The Rayleigh ratio, R_θ can be approximated and expressed by the averaged molecular weight (M_W), mean-square radius of gyration ($\langle R_g^2\rangle$), and second virial coefficient (A_2) as functions of c and q (defined as $\frac{4\pi n}{\lambda}\sin\frac{\theta}{2}$, where n is the refractive index of solution for light scattering).

$$\frac{K_c}{R_\theta} = \frac{1}{M_w}\left(1 + \frac{1}{3}\langle R_g^2\rangle q^2\right) + 2A_2 c$$

The optical constant $K \equiv 4\pi^2 n^2 (dn/dc)^2/N_A\lambda^4$, where dn/dc and N_A are the refractive index increment and Avogadro's number, respectively. Toluene ($R_{\theta,Tol} = 1 \times 10^{-5}$ cm^{-1}) was used as a standard and water as the solvent background.

3. RESULTS AND DISCUSSION

The amphiphilic BCP of PEO_{114}-b-$PTMSPMA_{228}$ was synthesized using bromine-ended PEO (PEO_{114}-Br, M_n = 5000 g/mol) as the macroinitiator through ATRP.[32−34] The polymerization was catalyzed by CuBr in anisole at 65 °C for 1.5 h. The repeating unit of the hydrophobic PTMSPMA block was calculated to be 228 using ^{1}H NMR while PEO serves as an internal standard (Figure S1). The dispersity (Đ) of the polymer is 1.3 based on the GPC measurement calibrated with PS. The self-assembly of PEO_{114}-b-$PTMSPMA_{228}$ was carried out in a water/ethanol mixture. In brief, water as a non-solvent for the PTMSPMA block was added to the BCP solution (10 mg mL^{-1} in ethanol) at a rate of ~80 μL per min. The final water concentration is around 54.5 vol %. After stirring for 0.5 h at room temperature, 0.2 mL of TEA was added to hydrolyze the PTMSPMA block to form hybrid micelles with a hydrophobic polysilsesquioxane core and a hydrophilic PEO shell.[32] The final micelles were dialyzed to remove ethanol and stored in water. In the absence of TEOS, PEO_{114}-b-$PTMSPMA_{228}$ formed spherical micelles, as confirmed by

https://doi.org/10.1021/acs.langmuir.1c01554
Langmuir 2021, 37, 9865−9872

electron microscopy (Figure 1a,b), since the amphiphilic BCP has a long PEO block.[23] TEM reveals the monodispersity of those spherical micelles with a diameter of 21.6 ± 2.8 nm (Figure 1c and Table 1), denoted Si-0 in Table 1. The size was confirmed by SAXS in solution (Figure 1g). The scattering profile shows a low q peak at 0.38 nm^{-1} and it fits well with the core-shell spherical model. The average size of nanospheres is 22 nm in solution, in good agreement with the TEM result.

With TEOS as a reactive addictive, we first examined whether TEOS would be incorporated in the hydrophobic PTMSPMA core. When the volume of TEOS (V_{TEOS}) was <0.23 mL in the total volume of ~4 mL (water/ethanol mixture), there was a continuous volume expansion with the increase of the TEOS concentration. The diameter of spherical micelles increased to 22.3 ± 2.5 nm with V_{TEOS} = 0.01 mL (Si-1 in Table 1). When V_{TEOS} reached 0.2 mL, much larger spherical micelles with an average diameter of 32.2 ± 4.1 nm were observed in TEM (Si-4, Figure 1d−f). There were few hollow aggregates observed for Si-4, likely indicating the formation of vesicles; however, they are far less, as compared to spherical micelles. The SAXS profile of Si-4 is given in Figure 1h. The scattering peak shifted to a lower q to 0.25 nm^{-1}, compared to that of Si-0 (Figure 1g), suggesting the size increase of the spherical micelles. The average size is about 34 nm, as estimated by SAXS, close to the result by TEM. These results suggest that TEOS hydrolyzed in the core of micelles, further resulting in the expansion of the hydrophobic core of micelles.

Furthermore, increasing V_{TEOS} would lead to morphological transitions as expected when increasing the hydrophobic-to-hydrophilic ratio. With V_{TEOS} above 0.27 mL, vesicles became the dominant nanostructures. These vesicles show a high electron contrast due to the formation of polysilsesquioxane. First of all, we confirmed the formation of vesicles in solution. At V_{TEOS} = 0.3 mL (Si-7), the representative electron microscopy results are given in Figure 2a,b. These vesicles show typical hollow-like structures with a wall thickness of 18.6 ± 1.9 nm (Figure 2c). Fairly uniform vesicles were seen under a transmission electron microscope with a diameter of 60.4 ± 7.0 nm. To confirm the formation vesicles in solution, we used light scattering to measure the ratio of root-mean-square radius of gyration $\langle R_g^2\rangle^{1/2}$ to hydrodynamic radius (R_h). The mean-square-root radius of gyration $\langle R_g^2\rangle^{1/2}$ was measured using Zimm plot analysis, as described in the Experimental Section (Figure 2d,e and Table S1). The value of $\langle R_g^2\rangle^{1/2}/R_h$ is characteristic for different morphologies in solution. In the absence of TEOS, spherical micelles of PEO_{114}-b-$PTMSPMA_{228}$ yield a $\langle R_g^2\rangle^{1/2}/R_h$ of 0.81 (Figure 2d), close to that of the homogeneous hard sphere ($\langle R_g^2\rangle^{1/2}/R_h$ = 0.775).

At V_{TEOS} = 0.3 mL (Si-7, Figure 2e), the $\langle R_g^2\rangle^{1/2}/R_h$ of ~1 suggests the formation of vesicles.

When V_{TEOS} is ≥0.35 mL, there are much larger structures formed since the solution became very milky after the addition of water. The aggregation of vesicles formed three-dimensional (3-D) complexes, also known as large compound vesicles from the membrane fusion of the overcrowded unilamellar vesicles.[35] These vesicles are usually bicontinuous, as observed in surfactants.[36] Figures 2f,g show the examples of large compound vesicles at V_{TEOS} = 0.5 and 0.8 mL. Although the walls are similar to that of the vesicles, these frameworks are obviously interconnected from bicontinuous structures with hollow interiors filled with hydrophilic PEO chains, appearing as the lighter region under a transmission electron microscope.

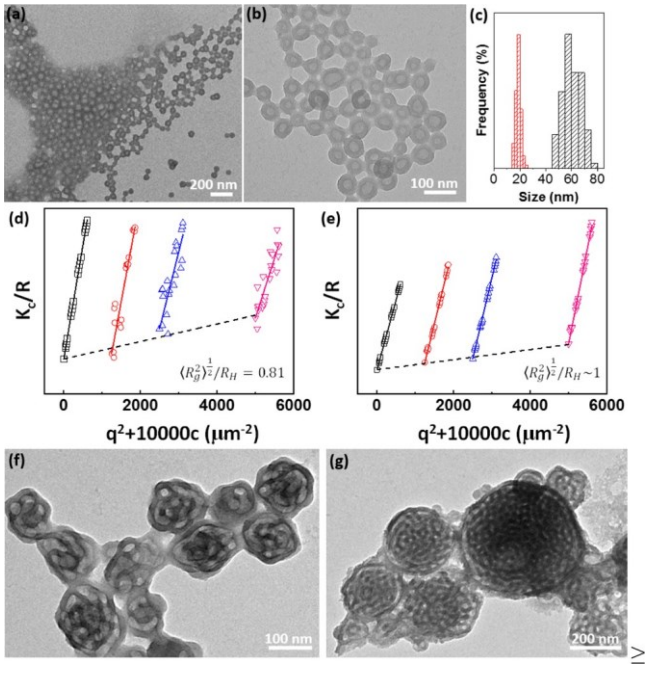

Figure 2. (a,b) TEM images of Si-7. (c) Wall thickness (red) and size distribution (black) of Si-7. Zimm plots of (d) Si-0 and (e) Si-7. TEM images of (f) Si-10 and (g) Si-12.

With a higher V_{TEOS} = 0.8 mL, the aggregates became much larger, and they also had some irregular shapes (Figures 2g and 3k−j). These aggregates were not stable in solution over time, and they would precipitate out when storing without stirring. The porosity within large compound vesicles, similar to those at V_{TEOS} = 0.5 mL, seemed to be disordered but interconnected.

Such structural evolution is summarized in Figure 3. Without varying the chemical composition, the assembly nanostructures of a micelle-forming BCP PEO_{114}-b-$PTMSPMA_{228}$ are clearly dominant by the TEOS concentration. These morphological transitions are aligned with the change in the hydrophobic-to-hydrophilic balance of amphiphilic BCPs or surfactants when increasing TEOS. As TEOS is hydrophobic and it does not dissolve in water, it is reasonable that the addition of TEOS would result in the swelling of hydrophobic cores. We plotted the diameter of spherical micelles as a function of V_{TEOS}, as shown in Figure 4. Interestingly, they are linearly correlated. In previous studies by Eisenberg,[10] the size of spherical micelles is determined by the block lengths of the two blocks. While PEO_{114}-b-$PTMSPMA_{228}$ has a defined composition in all cases, the PTMSPMA core is swollen by TEOS. Since the diameter is

https://doi.org/10.1021/acs.langmuir.1c01554
Langmuir 2021, 37, 9865−9872

linearly correlated with the volume of TOES, it is reasonable to conclude that TEOS is predominantly present in the core of micelles. The swelling may not vary the chain stretching ratio of the core-forming PTMSPMA,[10] although it increases the hydrophobic-to-hydrophilic ratio. The size of spherical micelles increased to 39.3 ± 5.9 nm at V_{TEOS} = 0.23 mL, as compared to 21.6 ± 2.8 nm in the absence of TEOS. This corresponds to the increase in the hydrophobic volume about six times, comparable to the volume of TEOS and the BCP. Swelling of the hydrophobic core would increase the packing parameter and eventually lead to a morphological transition.

After the formation of vesicles, there is a sudden change as comparing the dimension of micellar diameters with the wall

https://doi.org/10.1021/acs.langmuir.1c01554
Langmuir 2021, 37, 9865−9872

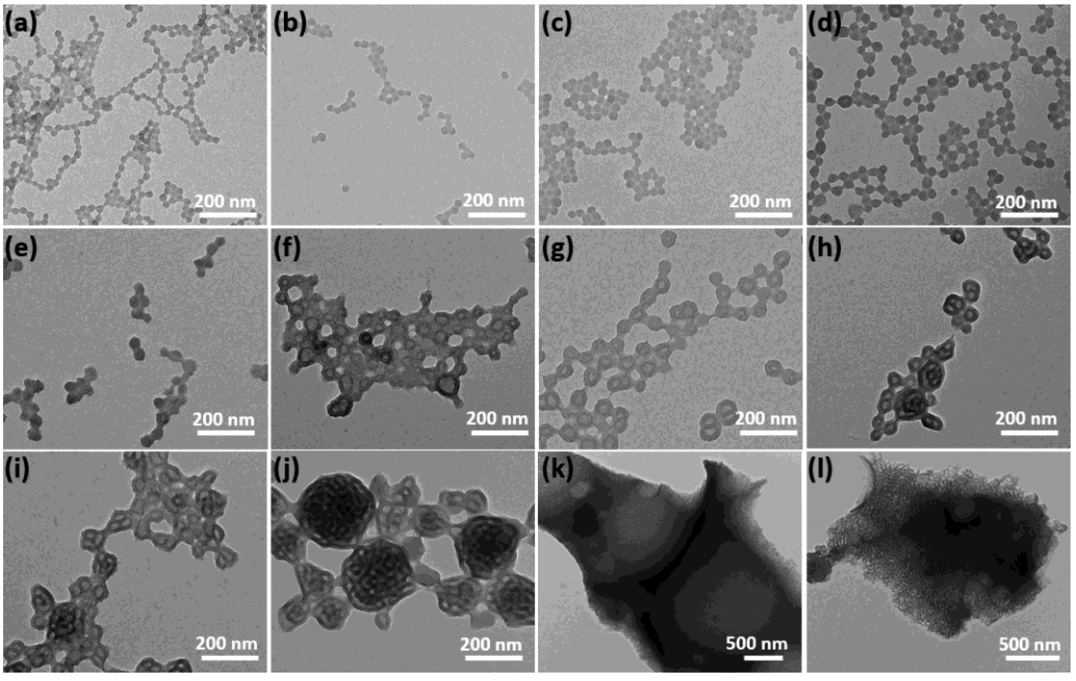

Figure 3. TEM images of Si-1 to Si-12 with the increase of TEOS amount. The morphology changed from micelles to vesicles and bicontinuous phase mesoporous structures with the increase of TEOS amount. The pore size and wall thickness histogram plots are summarized in Figure S2.

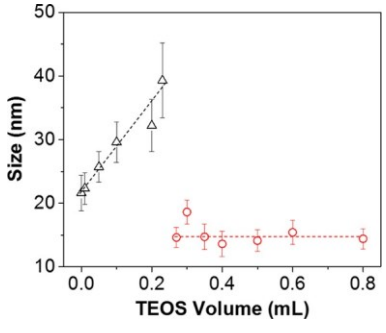

Figure 4. Diameter of polymer micelles (hollow black triangle) and wall thickness (hollow red circle) of bilayer vesicles at different TEOS volumes.

thickness. The wall thickness of these vesicles[35] seems to be independent of the concentration of TEOS. It is close to 15 nm with a minimum change with V_{TEOS}, as seen in Figure 4 and Table 1. The wall thickness of inner and outer membranes in large compound vesicles is uniform with a very low standard error. The wall thickness of vesicles is much smaller compared to the diameter of spherical micelles since the packing geometry of polymer chains is very different in the two types of nanostructures. The core-forming blocks are usually much less stretched in layered assemblies as compared to that in spherical micelles. As TEOS does not contribute to the wall thickness, it is presumed that TEOS would occupy the free volume and essentially swell laterally along the planar direction of the vesicle membrane (see below). The swelling would also cause the decrease of the hydrophilic PEO density per unit surface, eventually leading to the formation of large compound vesicles accompanied by the shrinkage of the interior similar to that of the large compound vesicles reported previously.[37] For example, at V_{TEOS} = 0.6 mL, the diameter of the "hollow" interior is 11.4 ± 1.9 nm, as measured by the gap between the walls.

These hybrid nanostructures are silica-rich, and they can be converted to inorganic silica upon thermal annealing to promote further condensation of polysilsesquioxane. The aqueous solution of aggregates was first dried through lyophilization. The as-resultant powders were further calcined at 550 °C for 2 h under air to remove all organic components. We characterized four samples after calcination using TEM, including Si-0, Si-4, Si-7, and Si-11. For spherical micelles of PEO_{114}-b-$PTMSPMA_{228}$ in the absence of TEOS, the spherical structures were barely preserved. The aggregation and sintering of spherical nanoparticles to form bulky structures are seen, likely due to the low content of silica components (see Figure S3). With V_{TEOS} = 0.2 mL, Si-4 was converted to spherical silica nanoparticles after calcination. With $V_{TEOS} \geq 0.2$ mL, the structural integrity can be retained after the removal of organic species. However, the particle size decreased significantly from 32.2 ± 4.1 to 17.0 ± 1.6 nm after calcination (Figure 5a,b). This corresponds to a volume shrinkage of 85.3%. With V_{TEOS} = 0.3 mL, Si-7 with vesicular structures became hollow silica nanoparticles. These hollow structures are uniform compared to that of the vesicles prior to calcination. It seems that hollow silica nanospheres were interconnected with a very thin silica layer. This is presumably because of the low hydrolysis degree of TEOS in the membrane of vesicles. The size shrinkage is much milder compared to that of spherical micelles. Hollow silica nanospheres show an average diameter of 53.1 ± 7.3 nm and a wall thickness of 11.1 ± 1.5 nm (Figure 5c,d). Unlike other reported hollow silica,[38,39] the shell of those hollow nanospheres has a typical bilayer structure. The formation of such bilayer silica structure is due to the hydrolysis of TEOS and the PTMSPMA block at the two interfaces (inner and outer) of the vesicle membrane and the solvent. This is reasonable because the hydrolysis occurs only in the presence of water and TEA. The wall thickness measured across the dark regions was close to that of the vesicles, suggesting that the

https://doi.org/10.1021/acs.langmuir.1c01554
Langmuir 2021, 37, 9865−9872

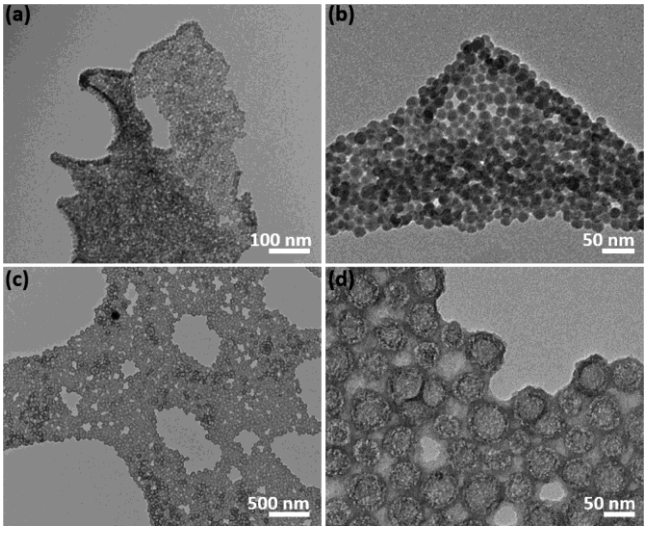

Figure 5. TEM images of (a,b) Si-4 and (c,d) Si-7 after calcination at 550 °C.

shrinkage across the membrane is low at a higher TEOS concentration.

With a much higher concentration of TEOS, the frameworks of bicontinuous large compound vesicles were well-preserved after calcination to form mesoporous silica. The example of Si-11 with V_{TEOS} = 0.6 mL is given in Figures 6a,b. The porous structures have a thick silica wall of 15.4 ± 1.9 nm, close to the wall thickness of large compound vesicles. The pores seem to be disordered but interconnected, like those of the vesicles. The size of the pore is around 12 nm measured from wall-to-wall using the TEM. The mesoporous silica was characterized via nitrogen sorption isotherms (Figure 6c). The Brunauer−Emmett−Teller specific surface area was calculated to be 474 $m^2\ g^{-1}$. Clear-type IV isotherms can be seen as an indication of the mesoporous feature, although it shows a large amount of micropores. The pore size was measured to be 11.6 nm (Figure 6d), close to the pore size obtained by TEM. Figures 6e,f show the SAXS data of Si-11 and porous materials, respectively. Both samples show a pseudo-Bragg peak, which shifts from 0.17 to 0.3 nm^{-1}. We are able to use a core-2-shell spherical model (form factor) combined with a hard-sphere structure factor (see Figure S4) to describe the SAXS data.[26] According to Babinet's principle, the core can represent empty pores with interconnected shells. The quasi-Bragg peaks presumably originate from the periodic spacing between the pores. The best-fit spacing derived from the hard-sphere structure factor yields ~36 and ~23 nm for Si-11 and porous materials of Si-11

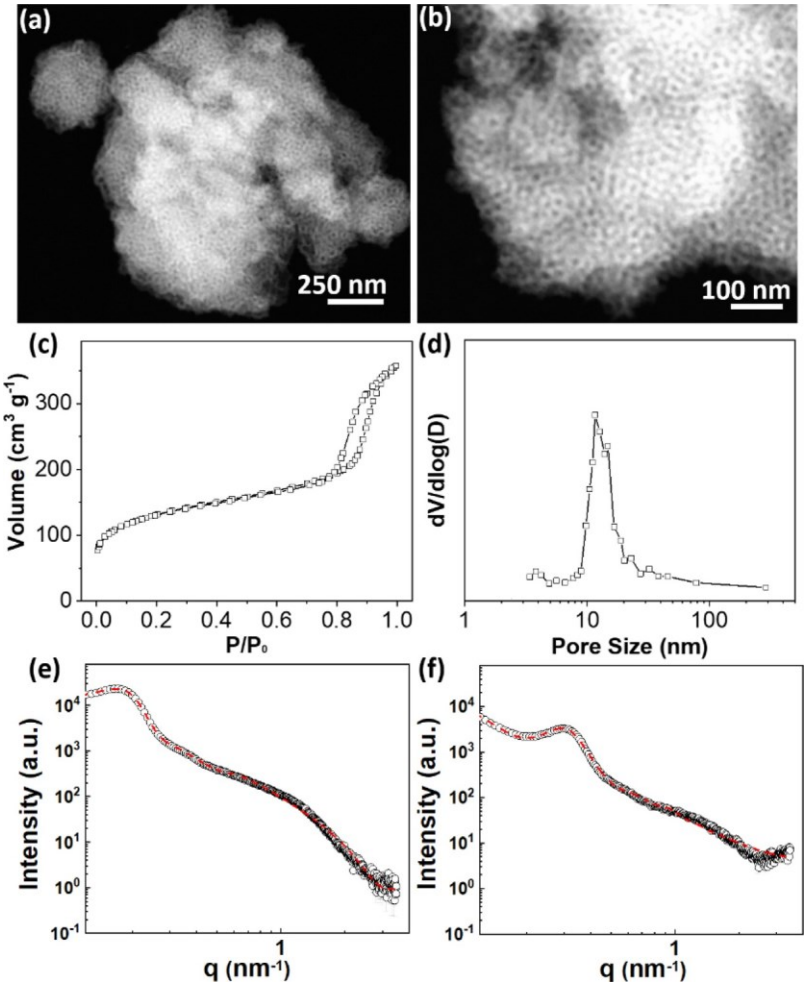

Figure 6. (a,b) Dark-field TEM images of mesoporous silica obtained from thermal calcination of Si-11. (c) N_2 sorption isotherms and (d) the corresponding size distribution of mesoporous silica. SAXS pattern of (e) Si-11 and (f) mesoporous silica.

https://doi.org/10.1021/acs.langmuir.1c01554
Langmuir 2021, 37, 9865−9872

after calcination, respectively, suggesting the shrinkage of frameworks (see the Supporting Information).

The mechanism of pore formation is quite different from other traditional methods such as precipitation synthesis or evaporation-induced self-assembly. At a dilute concentration of amphiphilic BCPs, the interaction between micelles is minimum. Our method features the co-assembly of amphiphilic BCPs with a reactive additive such as TEOS and the confined hydrolysis within the hydrophobic domains of polymer assemblies. Therefore, the frameworks of mesoporous silica are derived from the hydrophobic core of polymer assemblies where the hydrolysis of TEOS and PTMSPMA occurs. In addition to the formation of mesoporous structures, other nanostructures of polymer assemblies obtained at different TEOS concentrations, for example, nanospheres and hollow vesicles, can be converted to inorganic silica nanoparticles.

4. CONCLUSIONS

To summarize, we demonstrated a novel co-self-assembly strategy to control the self-assembly outcomes of a micelle-forming amphiphilic BCP of PEO_{114}-b-$PTMSPMA_{228}$. With a reactive additive, TEOS, PEO_{114}-b-$PTMSPMA_{228}$ was assembled into a variety of nanostructures in the mixture of water and ethanol. Hydrophobic TEOS was shown to swell the hydrophobic domains to vary the hydrophobic-to-hydrophilic balance of the amphiphilic BCPs. The assembly nanostructures depending on the amount of TEOS showed a continuous evolution from spherical micelles to vesicles and eventually to large compound vesicles. TEOS also reacted with the PTMSPMA block in the hydrolysis−condensation process to fix these nanostructures. With high TEOS concentrations, these polymer assemblies could be further converted into silica nanomaterials, including nanospheres, hollow nanoparticles with dual shells, and mesoporous frameworks. The method highlights the co-assembly of the amphiphilic BCP with the reactive additive that possibly opens a new door to control the self-assembly outcomes without additional syntheses as well as design porous nanostructures of other inorganic materials.

ASSOCIATED CONTENT

Supporting Information

The Supporting Information is available free of charge at https://pubs.acs.org/doi/10.1021/acs.langmuir.1c01554.

^{1}H NMR spectrum, GPC elution curve, additional electron microscopic images, additional SLS spectra, size distribution of polymer particles, and description of the core−shell model and the hard-sphere model (PDF)

AUTHOR INFORMATION

Corresponding Author

Jie He − Department of Chemistry and Polymer Program, Institute of Materials Science, University of Connecticut, Storrs, Connecticut 06269, United States; orcid.org/0000-0003-0252-3094; Email: jie.he@uconn.edu

Authors

Lei Jin − Department of Chemistry, University of Connecticut, Storrs, Connecticut 06269, United States; orcid.org/0000-0002-6070-7863

Chung-Hao Liu − Polymer Program, Institute of Materials Science, University of Connecticut, Storrs, Connecticut 06269, United States

Daniel Cintron − Department of Chemistry, University of Connecticut, Storrs, Connecticut 06269, United States

Qiang Luo − Department of Chemistry, University of Connecticut, Storrs, Connecticut 06269, United States

Mu-Ping Nieh − Polymer Program, Institute of Materials Science and Department of Chemical & Biomolecular Engineering, University of Connecticut, Storrs, Connecticut 06269, United States; orcid.org/0000-0003-4462-8716

Complete contact information is available at: https://pubs.acs.org/10.1021/acs.langmuir.1c01554

Notes

The authors declare no competing financial interest.

ACKNOWLEDGMENTS

J.H. is grateful for the financial support of the National Science Foundation (CBET 1705566). SAXS data were collected on a Bruker Nano STAR supported by NSF-MRI (MRI-1228817). TEM studies were performed using the facilities in the UConn/Thermo Fisher Scientific Center for Advanced Microscopy and Materials Analysis (CAMMA). This work was also partially supported by the Green Emulsions, Micelles, and Surfactants (GEMS) Center.

REFERENCES

(1) Mai, Y.; Eisenberg, A. Self-assembly of block copolymers. Chem. Soc. Rev. 2012, 41, 5969−5985.

(2) Yang, P.; Deng, T.; Zhao, D.; Feng, P.; Pine, D.; Chmelka, B. F.; Whitesides, G. M.; Stucky, G. D. Hierarchically Ordered Oxides. Science 1998, 282, 2244−2246.

(3) Wan, Y.; Zhao, D. On the Controllable Soft-Templating Approach to Mesoporous Silicates. Chem. Rev. 2007, 107, 2821−2860.

(4) Zhang, L.; Jin, L.; Liu, B.; He, J. Templated Growth of Crystalline Mesoporous Materials: From Soft/Hard Templates to Colloidal Templates. Front. Chem. 2019, 7, 22.

(5) Liang, C.; Li, Z.; Dai, S. Mesoporous Carbon Materials: Synthesis and Modification. Angew. Chem., Int. Ed. 2008, 47, 3696−3717.

(6) Kipkemboi, P.; Fogden, A.; Alfredsson, V.; Flodström, K. Triblock Copolymers as Templates in Mesoporous Silica Formation: Structural Dependence on Polymer Chain Length and Synthesis Temperature. Langmuir 2001, 17, 5398−5402.

(7) Soler-Illia, G. J. d. A. A.; Crepaldi, E. L.; Grosso, D.; Sanchez, C. Block copolymer-templated mesoporous oxides. Curr. Opin. Colloid Interface Sci. 2003, 8, 109−126.

(8) Wen, W.; Guan, S.; Yang, Z.; Chen, A. Inverse Bicontinuous Structure by Polymerization-Induced Self-Assembly Against Single-Chain Nanoparticles. ACS Macro Lett. 2021, 10, 603−608.

(9) Zhang, L.; Eisenberg, A. Multiple Morphologies of "Crew-Cut" Aggregates of Polystyrene-b-poly(acrylic acid) Block Copolymers. Science 1995, 268, 1728−1731.

(10) Zhang, L.; Eisenberg, A. Formation of crew-cut aggregates of various morphologies from amphiphilic block copolymers in solution. Polym. Adv. Technol. 1998, 9, 677−699.

(11) Zhang, L.; Yu, K.; Eisenberg, A. Ion-Induced Morphological Changes in "Crew-Cut" Aggregates of Amphiphilic Block Copolymers. Science 1996, 272, 1777−1779.

(12) Tanaka, H.; Hasegawa, H.; Hashimoto, T. Ordered structure in mixtures of a block copolymer and homopolymers. 1. Solubilization of low molecular weight homopolymers. Macromolecules 1991, 24, 240−251.

(13) Ruan, Y.; Gao, L.; Yao, D.; Zhang, K.; Zhang, B.; Chen, Y.; Liu, C.-Y. Polymer-Grafted Nanoparticles with Precisely Controlled Structures. ACS Macro Lett. 2015, 4, 1067−1071.
(14) Dobrosielska, K.; Wakao, S.; Suzuki, J.; Noda, K.; Takano, A.; Matsushita, Y. Effect of Homopolymer Molecular Weight on Nanophase-Separated Structures of AB Block Copolymer/C Homopolymer Blends with Hydrogen-Bonding Interactions. Macromolecules 2009, 42, 7098−7102.
(15) Lin, Y.; Daga, V. K.; Anderson, E. R.; Gido, S. P.; Watkins, J. J. Nanoparticle-Driven Assembly of Block Copolymers: A Simple Route to Ordered Hybrid Materials. J. Am. Chem. Soc. 2011, 133, 6515−6516.
(16) Liu, Y.; Li, Y.; He, J.; Duelge, K. J.; Lu, Z.; Nie, Z. Entropy-Driven Pattern Formation of Hybrid Vesicular Assemblies Made from Molecular and Nanoparticle Amphiphiles. J. Am. Chem. Soc. 2014, 136, 2602−2610.
(17) Zhu, J.; Yu, H.; Jiang, W. Morphological Transition of Aggregates from ABA Amphiphilic Triblock Copolymer Induced by Hydrogen Bonding. Macromolecules 2005, 38, 7492−7501.
(18) Vukovic, I.; ten Brinke, G.; Loos, K. Hexagonally Perforated Layer Morphology in PS-b-P4VP(PDP) Supramolecules. Macromolecules 2012, 45, 9409−9418.
(19) Ikkala, O.; ten Brinke, G. Functional Materials Based on Self-Assembly of Polymeric Supramolecules. Science 2002, 295, 2407−2409.
(20) Zhang, L.; Eisenberg, A. Multiple Morphologies and Characteristics of "Crew-Cut" Micelle-like Aggregates of Polystyrene-b-poly(acrylic acid) Diblock Copolymers in Aqueous Solutions. J. Am. Chem. Soc. 1996, 118, 3168−3181.
(21) Xu, J.; Yang, Y.; Wang, K.; Li, J.; Zhou, H.; Xie, X.; Zhu, J. Additives Induced Structural Transformation of ABC Triblock Copolymer Particles. Langmuir 2015, 31, 10975−10982.
(22) Hu, Y.; Chen, Y.; Du, J. Evolution of diverse higher-order membrane structures of block copolymer vesicles. Polym. Chem. 2019, 10, 3020−3029.
(23) Du, J.; Chen, Y. Atom-Transfer Radical Polymerization of a Reactive Monomer: 3-(Trimethoxysilyl)propyl Methacrylate. Macromolecules 2004, 37, 6322−6328.
(24) Du, J.; Chen, Y. Organic-Inorganic Hybrid Nanoparticles with a Complex Hollow Structure. Angew. Chem., Int. Ed. 2004, 43, 5084−5087.
(25) Du, J.; Chen, Y. Preparation of Organic/Inorganic Hybrid Hollow Particles Based on Gelation of Polymer Vesicles. Macromolecules 2004, 37, 9710−9716.
(26) Jin, L.; Su, X.; Shi, J.; Shih, K. C.; Cintron, D.; Cai, T.; Nieh, M. P.; Chen, O.; Suib, S. L.; Jain, M.; He, J. Crystalline Mesoporous Complex Oxides: Porosity-Controlled Electromagnetic Response. Adv. Funct. Mater. 2020, 30, 1909491.
(27) Jin, L.; Liu, B.; Louis, M. E.; Li, G.; He, J. Highly Crystalline Mesoporous Titania Loaded with Monodispersed Gold Nanoparticles: Controllable Metal−Support Interaction in Porous Materials. ACS Appl. Mater. Interfaces 2020, 12, 9617−9627.
(28) Hu, M.; Jin, L.; Su, X.; Bamonte, S.; Lu, X.; Gao, P.; Suib, S. L.; Liu, B.; He, J. Polymer-Assisted Co-Assembly towards Synthesis of Mesoporous Titania Encapsulated Monodisperse PdAu for Highly Selective Hydrogenation of Phenylacetylene. ChemCatChem 2020, 12, 1476−1482.
(29) Hu, M.; Jin, L.; Dang, Y.; Suib, S. L.; He, J.; Liu, B. Supported Pt Nanoparticles on Mesoporous Titania for Selective Hydrogenation of Phenylacetylene. Front. Chem. 2020, 8, 581512.
(30) Liu, B.; Jin, L.; Zheng, H.; Yao, H.; Wu, Y.; Lopes, A.; He, J. Ultrafine Co-based Nanoparticle@Mesoporous Carbon Nanospheres toward High-Performance Supercapacitors. ACS Appl. Mater. Interfaces 2017, 9, 1746−1758.
(31) Liu, B.; Yao, H.; Daniels, R. A.; Song, W.; Zheng, H.; Jin, L.; Suib, S. L.; He, J. A facile synthesis of Fe, carbon nitride nanospheres with superior electrocatalytic activity. Nanoscale 2016, 8, 5441−5445.
(32) Liu, B.; Luo, Z.; Federico, A.; Song, W.; Suib, S. L.; He, J. Colloidal Amphiphile-Templated Growth of Highly Crystalline Mesoporous Nonsiliceous Oxides. Chem. Mater. 2015, 27, 6173−6176.
(33) Li, W.; Kuo, C.-H.; Kanyo, I.; Thanneeru, S.; He, J. Synthesis and Self-Assembly of Amphiphilic Hybrid Nano Building Blocks via Self-Collapse of Polymer Single Chains. Macromolecules 2014, 47, 5932−5941.
(34) Du, J.; Chen, Y. Hairy Nanospheres by Gelation of Reactive Block Copolymer Micelles. Macromol. Rapid Commun. 2005, 26, 491−494.
(35) Shen, H.; Eisenberg, A. Morphological Phase Diagram for a Ternary System of Block Copolymer PS310-b-PAA52/Dioxane/H2O. J. Phys. Chem. B 1999, 103, 9473−9487.
(36) Yang, Y.; Yao, H.; Hong, M. Distinguishing Bicontinuous Lipid Cubic Phases from Isotropic Membrane Morphologies Using 31P Solid-State NMR Spectroscopy. J. Phys. Chem. B 2013, 117, 4993−5001.
(37) Zhang, L.; Eisenberg, A. Morphogenic Effect of Added Ions on Crew-Cut Aggregates of Polystyrene-b-poly(acrylic acid) Block Copolymers in Solutions. Macromolecules 1996, 29, 8805−8815.
(38) Zhang, T.; Zhang, Q.; Ge, J.; Goebl, J.; Sun, M.; Yan, Y.; Liu, Y.-s.; Chang, C.; Guo, J.; Yin, Y. A Self-Templated Route to Hollow Silica Microspheres. J. Phys. Chem. C 2009, 113, 3168−3175.
(39) Du, J.; Chen, Y.; Zhang, Y.; Han, C. C.; Fischer, K.; Schmidt, M. Organic/Inorganic Hybrid Vesicles Based on A Reactive Block Copolymer. J. Am. Chem. Soc. 2003, 125, 14710−14711.

https://doi.org/10.1021/acs.langmuir.1c01554
Langmuir 2021, 37, 9865−9872